

A possible way to achieve anomalous valley Hall effect by piezoelectric effect in GdCl_2 monolayer

San-Dong Guo¹, Jing-Xin Zhu¹, Wen-Qi Mu¹ and Bang-Gui Liu^{2,3}

¹*School of Electronic Engineering, Xi'an University of Posts and Telecommunications, Xi'an 710121, China*

²*Beijing National Laboratory for Condensed Matter Physics, Institute of Physics, Chinese Academy of Sciences, Beijing 100190, People's Republic of China and*

³*School of Physical Sciences, University of Chinese Academy of Sciences, Beijing 100190, People's Republic of China*

Ferrovalley materials can achieve manipulation of the valley degree of freedom with intrinsic spontaneous valley polarization introduced by their intrinsic ferromagnetism. A good ferrovalley material should possess perpendicular magnetic anisotropy (PMA), valence band maximum (VBM)/conduction band minimum (CBM) at valley points, strong ferromagnetic (FM) coupling and proper valley splitting. In this work, the monolayer GdCl_2 is proposed as a potential candidate material for valleytronic applications by the first-principles calculations. It is proved that monolayer GdCl_2 is a FM semiconductor with the easy axis along out of plane direction and strong FM coupling. A spontaneous valley polarization with a valley splitting of 42.3 meV is produced due to its intrinsic ferromagnetism and spin orbital coupling (SOC). Although the VBM of unstrained monolayer GdCl_2 is away from valley points, a very small compressive strain (about 1%) can make VBM move to valley points. We propose a possible way to realize anomalous valley Hall effect in monolayer GdCl_2 by piezoelectric effect, not an external electric field, namely piezoelectric anomalous valley Hall effect (PAVHE). This phenomenon could be classified as piezo-valleytronics, being similar to piezotronics and piezophototronics. The only independent piezoelectric strain coefficient d_{11} is -2.708 pm/V, which is comparable to one of classical bulk piezoelectric material α -quartz ($d_{11}=2.3$ pm/V). The biaxial in-plane strain and electronic correlation effects are considered to confirm the reliability of our results. Finally, the monolayer GdF_2 is predicted to be a ferrovalley material with dynamic and mechanical stabilities, PMA, VBM at valley points, strong FM coupling, valley splitting of 47.6 meV, and d_{11} of 0.584 pm/V. Our works provide a possible way to achieve anomalous valley Hall effect by piezoelectric effect, which may stimulate further experimental works related with valleytronics.

PACS numbers: 71.20.-b, 77.65.-j, 72.15.Jf, 78.67.-n

Email:sandongyuwang@163.com

Keywords: Valleytronics, Ferromagnetism, Piezoelectronics, 2D materials

I. INTRODUCTION

Rather than spin and charge, carriers in crystals are also endowed with the valley degree of freedom, which is useful to process information and perform logic operations (valleytronics)¹⁻⁶. Two or more local energy extremes in the conduction band or valence band, which are degenerate but inequivalent at the inequivalent k points in the momentum space, are needed for a valley material. To realize applications of valleytronics, the electrons or holes in different valleys must be selectively produced or manipulated. Although the possibility to achieve manipulation of the valley degree of freedom has been proposed in certain three-dimensional (3D) materials⁷, the field of valleytronics is truly flourishing with the advent of two-dimensional (2D) materials.

The reduction in dimensionality of 2D materials results in that space inversion symmetry is often eliminated in 2D structures, allowing these materials to become piezoelectric⁸, which is also very important for valleytronics described by Berry curvature $\Omega(k)$. In 2D hexagonal systems with broken space inversion symmetry, the Berry curvature in the K and -K valleys will be nonzero along the out of plane direction, and the Berry curvatures of two valleys are in opposite signs. If the time reversal symmetry is also broken, their abso-

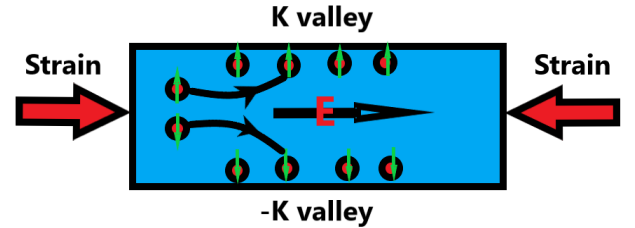


FIG. 1. (Color online) Sketch of anomalous valley Hall effect under an in-plane longitudinal electric field E , and the E is induced with uniaxial strain by piezoelectric effect. Upward arrows and downward arrows represent spin-up and spin-down carriers, respectively. Only one edge of the sample can accumulate the charge carriers, and another edge will accumulate ones, when reversing the magnetization orientation.

lute values are no longer identical, and the valley contrasting feature will be induced. Under an in-plane longitudinal electric field E , the Bloch electrons in these 2D systems will acquire an anomalous Hall velocity v due to $v \sim E \times \Omega(k)$ ⁹, and then the anomalous valley Hall effect will be produced, which can be achieved in ferrovalley materials¹⁰. Many ferrovalley materials have been predicted, such as 2H-VSe_2 ¹⁰, CrSi_2X_4 ($\text{X}=\text{N}$ and P)¹¹, VAgP_2Se_6 ¹², LaBr_2 ^{13,14}, VSi_2P_4 ¹⁵, NbX_2 ($\text{X}=\text{S}$

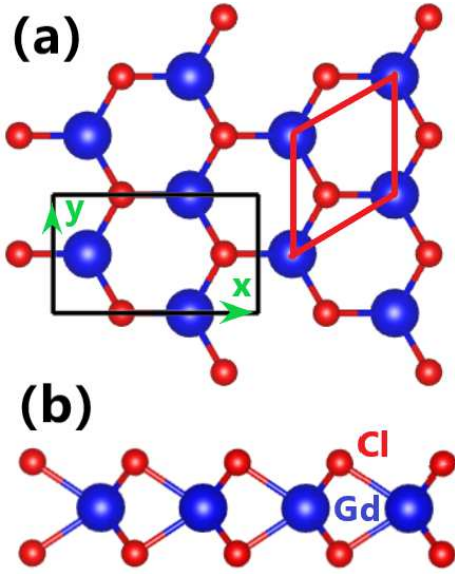


FIG. 2. (Color online) The (a) top view and (b) side view of crystal structure of monolayer GdCl_2 . The red and black frames represent the rhombus primitive cell and rectangle supercell. The rectangle supercell is used to calculate the piezoelectric stress coefficients, whose width and height are defined as x and y directions, respectively.

and Se)¹⁶, Nb_3I_8 ¹⁷, TiVI_6 ¹⁸. It is a natural idea to induce in-plane longitudinal electric field E with an applied uniaxial in-plane strain by piezoelectric effect, and then anomalous valley Hall effect can be produced, which is illustrated in Figure 1.

To well achieve PAVHE, a 2D material should possess the strong FM coupling with PMA (The out-of-plane magnetization easy axis is important not only for FM order but also for valley behavior.), the appropriate energy band gap and valley splitting (The band gap and valley splitting should be large enough to overcome the thermal noise.), and the pure in-plane piezoelectric effect with only d_{11} (The only independent d_{11} means only in-plane longitudinal electric field.). Recently, a kind of exotic 2D ferromagnetic semiconductors GdX_2 ($\text{X}=\text{Cl}, \text{Br}$ and I) based on rare-earth ions with f -electrons are predicted to have a large magnetization with high Curie temperature beyond 220 K^{19,20}. The monolayer GdI_2 is predicted as a promising candidate material for valleytronic applications, which is spontaneously valley polarized with a giant splitting of 149 meV²¹. However, GdI_2 possesses in-plane magnetic anisotropy, not PMA^{19,20}. Among GdX_2 ($\text{X}=\text{Cl}, \text{Br}$ and I) monolayers, the easy axis of only monolayer GdCl_2 is along the out of plane direction²⁰. The monolayer GdCl_2 has $\bar{p}6m2$ point-group symmetry, which means that only independent d_{11} is nonzero.

In light of PMA and independent d_{11} , monolayer GdCl_2 is likely to be a potential ferrovalley material to realize PAVHE. In this work, we investigate the valley physics and piezoelectric properties of monolayer GdCl_2 by the first-principles calculations. The monolayer GdCl_2

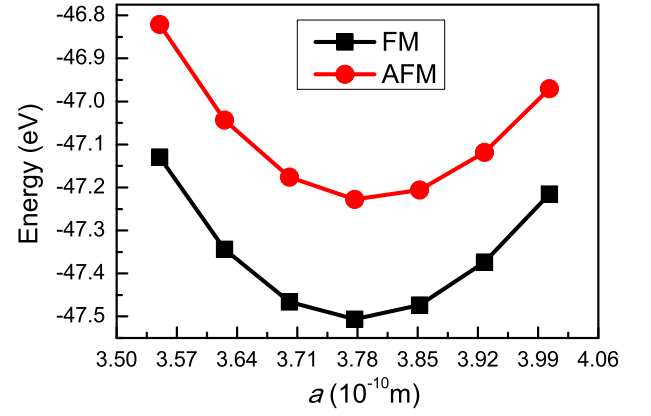


FIG. 3. (Color online) Calculated energy of AFM state and FM state of monolayer GdCl_2 as a function of lattice constants a with rectangle supercell.

exhibits a pair of valleys in the valence band at the K and -K points with a valley splitting of 42.3 meV due to its intrinsic ferromagnetism and SOC. The predicted d_{11} is -2.708 pm/V, which is comparable to one of α -quartz ($d_{11}=2.3$ pm/V). To confirm the reliability of our results, the biaxial in-plane strain and electronic correlation effects on valley physics and piezoelectric properties are considered. Finally, the monolayer GdF_2 is predicted to be likely to be a potential ferrovalley material. Our works provide potential 2D valleytronic materials to achieve PAVHE for developing high-performance and controllable valleytronics.

The rest of the paper is organized as follows. In the next section, we shall give our computational details and methods. In the next few sections, we shall present structure and stability, electronic structure and valley Hall effect, and piezoelectric properties of monolayer GdCl_2 , along with strain and electronic correlation effects on its valleytronic and piezoelectric properties. Finally, we shall give our discussion and conclusions.

II. COMPUTATIONAL DETAIL

First-principles calculations with spin-polarization are performed within density functional theory (DFT)²², as implemented in the Vienna Ab Initio Simulation Package (VASP)²³⁻²⁵ within the projector augmented-wave (PAW) method. The generalized gradient approximation (GGA) in the form of the Perdew-Burke-Ernzerhof (PBE) functional is used as the exchange-correlation interactions. The kinetic energy cutoff is set to 500 eV, and the total energy convergence criterion 10^{-8} eV is used. The optimized convergence criterion for atomic coordinates is less than $0.0001 \text{ eV} \cdot \text{\AA}^{-1}$ for force on each atom. The vacuum space is set to more than 18 \AA to avoid adjacent interactions. The $18 \times 18 \times 1$ Monkhorst-Pack k -point mesh is used to sample the Brillouin zone for calculating electronic structures and elastic properties,

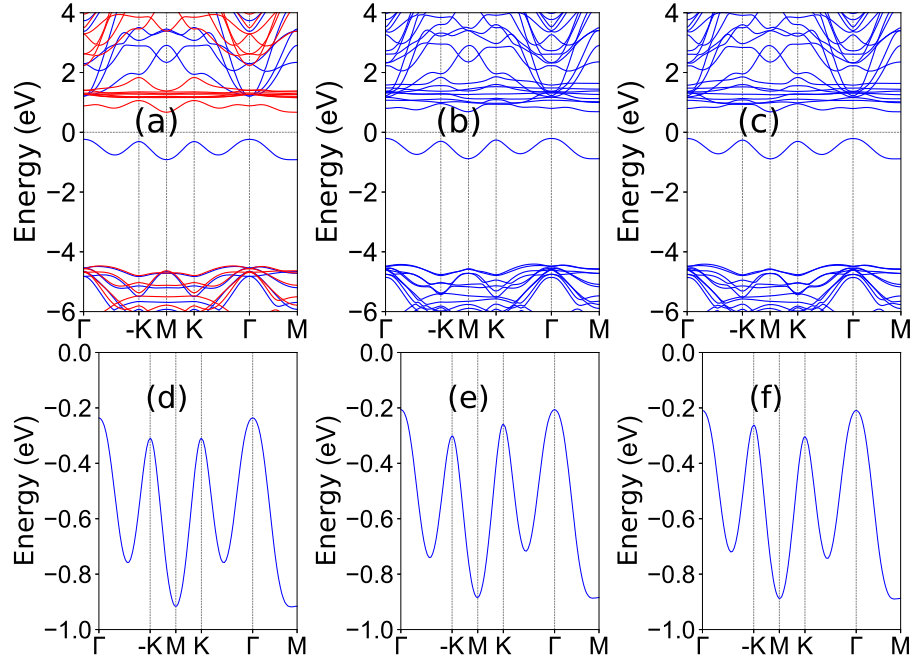


FIG. 4. (Color online) The band structure of monolayer GdCl₂ (a) without SOC; (b) and (c) with SOC for magnetic moment of Gd along the positive and negative z direction (out of plane), respectively. The (d), (e) and (f) are enlarged views of the valence bands near the Fermi level for (a), (b) and (c).

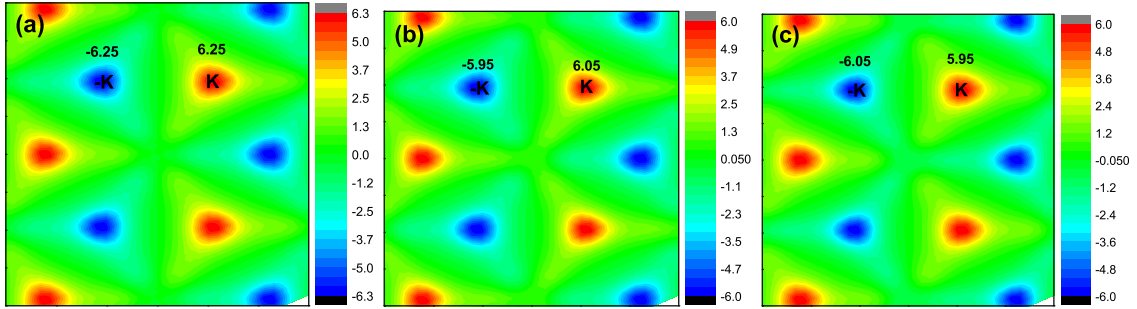


FIG. 5. (Color online) Calculated Berry curvature distribution of monolayer GdCl₂ in the 2D Brillouin zone (a) without SOC; (b) and (c) with SOC for magnetic moment of Gd along the positive and negative z direction (out of plane), respectively.

and $10 \times 20 \times 1$ Monkhorst-Pack k-point mesh for piezoelectric calculations. To account for the localized nature of $4f$ orbitals of Gd atoms, a Hubbard correction U_{eff} is employed within the rotationally invariant approach proposed by Dudarev et al., where U_{eff} is set as 4 eV, 5 eV, 8 eV^{19,20} for monolayer GdCl₂, GdBr₂ and GdI₂, respectively. The SOC is incorporated for self-consistent energy and band structure calculations. The elastic stiffness tensor C_{ij} are calculated by using strain-stress relationship (SSR) with GGA, and the piezoelectric stress tensor e_{ij} are carried out by density functional perturbation theory (DFPT) method²⁷ with GGA. The 2D elastic coefficients C_{ij}^{2D} and piezoelectric stress coefficients e_{ij}^{2D} have been renormalized by $C_{ij}^{2D} = L_z C_{ij}^{3D}$ and $e_{ij}^{2D} = L_z e_{ij}^{3D}$, where the L_z is the length of unit cell along z direction. Within finite displacement method, the in-

teratomic force constants (IFCs) of monolayer GdF₂ are calculated based on the $5 \times 5 \times 1$ supercell with FM ground state. Based on the harmonic IFCs, phonon dispersion spectrum of monolayer GdF₂ is obtained by the Phonopy code²⁸.

III. STRUCTURE AND STABILITY

The monolayer GdCl₂ belongs to the hexagonal crystal system with 2H-MoS₂ type structure, which contains one Gd atomic layer, sandwiched by two Cl atomic layers (See Figure 2). The corresponding point group is $\bar{p}6m2$ with broken inversion symmetry. The magnetic ground state of monolayer GdCl₂ is determined by comparing the energies of antiferromagnetic (AFM) and FM states

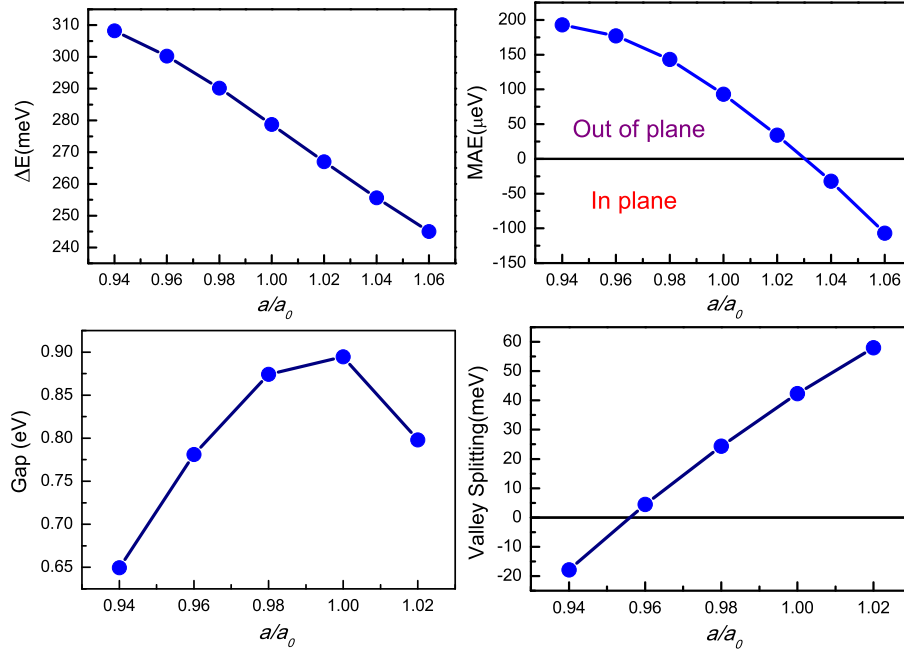


FIG. 6. (Color online) (Top left) The energy difference between the AFM and FM states (ΔE); (Top right) MAE; (Bottom left) energy band gap (Gap); (Bottom right) valley splitting as a function of the applied biaxial strain a/a_0 for monolayer GdCl_2 .

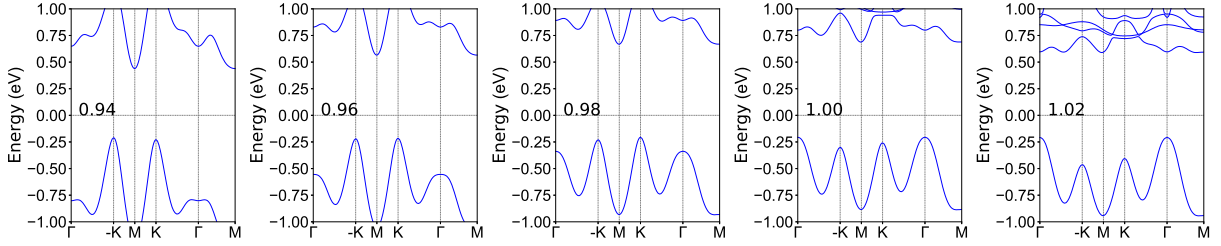


FIG. 7. (Color online) The energy band structures of monolayer GdCl_2 with a/a_0 from 0.94 to 1.02 by using GGA+SOC.

with rectangle supercell, which is shown in Figure 3. Calculated results show that the FM order is the most stable magnetic state, and the optimized lattice constants with FM order is 3.78 Å, which is consist with the reported value²⁰. Magnetic anisotropy plays a important role to realize the long-range magnetic ordering in 2D materials, which can be described by magnetic anisotropy energy (MAE). The monolayer GdBr_2 and GdI_2 possess in-plane magnetic anisotropy^{19,20}. This means that the spin orientations of Gd atoms can be random, and it is difficult to realize the long-range magnetic ordering without external field. However, the easy axis of monolayer GdCl_2 is along out of plane direction²⁰. By considering SOC interaction, the MAE of monolayer GdCl_2 is calculated as the difference between the in-plane and out-of-plane magnetization stability energy, and the corresponding value is 93 $\mu\text{eV}/\text{Gd}$.

The thermal and dynamic stabilities of monolayer GdCl_2 have been proved by Ab initio molecular dynamics (AIMD) simulations and phonon dispersion²⁰. It is also important to check the mechanical stability of monolayer

GdCl_2 by calculating elastic constants. Using Voigt notation, the elastic tensor C with $p6m2$ point-group symmetry for 2D materials can be reduced into:

$$C = \begin{pmatrix} C_{11} & C_{12} & 0 \\ C_{12} & C_{11} & 0 \\ 0 & 0 & (C_{11} - C_{12})/2 \end{pmatrix} \quad (1)$$

The calculated results show that C_{11} and C_{12} are 45.95 Nm^{-1} and 13.53 Nm^{-1} , respectively. The calculated C_{ij} satisfy the Born criteria of mechanical stability²⁹: $C_{11} > 0$ and $C_{11} - C_{12} > 0$, which confirms the mechanical stability of monolayer GdCl_2 . Due to hexagonal symmetry, the monolayer GdCl_2 is mechanically isotropic. The 2D Youngs moduli C^{2D} , shear modulus G^{2D} and Poisson's ratios ν^{2D} can simply be expressed as²⁹:

$$C^{2D} = \frac{C_{11}^2 - C_{12}^2}{C_{11}} \quad (2)$$

$$G^{2D} = C_{66} = \frac{C_{11} - C_{12}}{2} \quad (3)$$

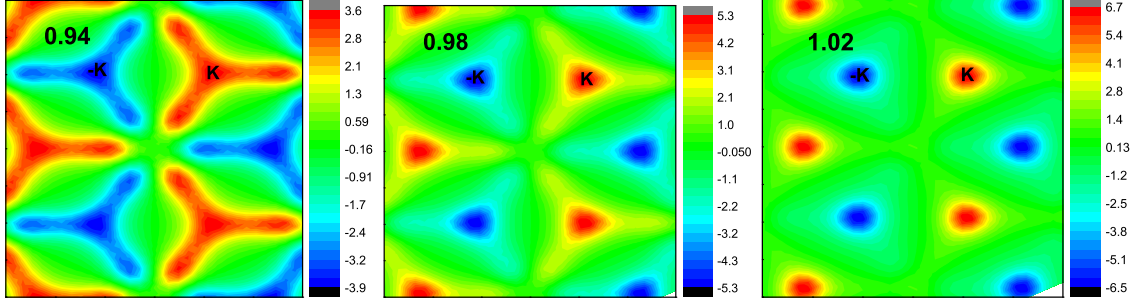


FIG. 8. (Color online) Calculated Berry curvature distribution of monolayer GdCl₂ in the 2D Brillouin zone with a/a_0 being 0.94, 0.98 and 1.02 by using GGA+SOC.

$$\nu^{2D} = \frac{C_{12}}{C_{11}} \quad (4)$$

The calculate Young's moduli C_{2D} , shear modulus G_{2D} and Poisson's ratio ν are 41.97 Nm⁻¹, 16.21 Nm⁻¹ and 0.295, respectively. The C_{2D} is less than that of graphene (340 Nm⁻¹)³⁰, which indicates that monolayer GdCl₂ can be easily tuned by strain, being favorable for novel flexible piezotronics.

IV. ELECTRONIC STRUCTURE AND VALLEY HALL EFFECT

The electronic configuration of isolated Gd atom is $4f^7 5d^1 6s^2$. For monolayer GdCl₂, two electrons of one Gd atom are transferred to the six neighboring I atoms, and the electronic configuration of Gd becomes $4f^7 5d^1$, which will introduce an $8 \mu_B$ magnetic moment. The calculated magnetic moment of Gd is $7.463 \mu_B$, and the total magnetic moment per unitcell is $8 \mu_B$. The spin-polarized band structure of monolayer GdCl₂ without SOC is shown in Figure 4. The calculated results show that the monolayer GdCl₂ is a semiconductors with an indirect band gap of 0.91 eV. The VBM and CBM are provided by the majority spins and minority spins, and they locate at the Γ and M high symmetry points, respectively. This makes monolayer GdCl₂ to be a bipolar magnetic semiconductor, which can generate 100 % spin-polarized currents with inverse spin-polarization direction for electron or hole doping. It is clearly seen that the energy extremes of K and -K high-symmetry points are degenerate in the valence band (Figure 4 (d)), and monolayer GdCl₂ is a potential ferrovalley material.

The band structures of monolayer GdCl₂ with SOC for magnetic moment of Gd along the positive and negative z direction (out of plane) are also plotted in Figure 4. When the SOC is included, the degeneracy between the K and -K valley states is removed in the valence band, and a spontaneous valley polarization is induced with valley splitting of 42.3 meV, which is higher than or compared to ones of reported ferrovalley materials, such as VAgP₂Se₆ (15 meV)¹², LaBr₂ (33 meV)^{13,14}, TiVI₆ (22 meV)¹⁸, VS₂P₄ (49.4 meV)¹⁵ and 2H-VSe₂ (89 meV)¹⁰.

It is found that the energy of K valley state is higher than one of -K valley (Figure 4 (e)). It is interesting that an external magnetic field can tune valley polarization of monolayer GdCl₂. By reversing the magnetization of Gd atoms, the spin and valley polarization can be flipped simultaneously, and the energy of -K valley becomes higher than one of K valley (Figure 4 (f)). These mean that manipulating magnetization direction is an efficient way to tune the valley properties of the monolayer GdCl₂. Furthermore, the band related with valley properties is separated well from other energy bands. Although the VBM of monolayer GdCl₂ occurs at Γ point, the K/-K valleys are still well defined and not far in energy. In fact, very small compressive strain (about 1%) can change VBM from Γ to K/-K point (next section). As is well known, the GGA overestimates the lattice constants of materials, and the VBM of monolayer GdCl₂ may intrinsically locate at K/-K point.

The combined effects of the intrinsic magnetic exchange field and strong SOC give rise to the spontaneous valley polarization. When the spin polarization is performed without SOC, the spin-up and spin-down states are completely split by the magnetic exchange interaction, but the energy extremes of K and -K high-symmetry points are degenerate in the valence band. When the magnetic exchange interaction is absent, SOC still can induce spin nondegeneracy at both K and -K valley due to missing spatial inversion symmetry, but K and -K valleys are energetically degenerate with opposite spins because of existing time reversal symmetry. In a word, combined with high Curie temperature (224 K)²⁰ and PMA, GdCl₂ is an ideal ferrovalley material for the valleytronic devices.

The valley Hall effect can be described by Berry curvature, and a nonzero Berry curvature along the out of plane direction can be attained in the K and -K valleys for hexagonal systems with broken space inversion symmetry. With the missing time reversal symmetry, the valley contrasting feature can be produced. To study these properties of monolayer GdCl₂, the Berry curvature is calculated directly from the calculated wave functions by using the VASPBERRY code, which is based on Fukui's method³¹. The calculated Berry curvature distribution

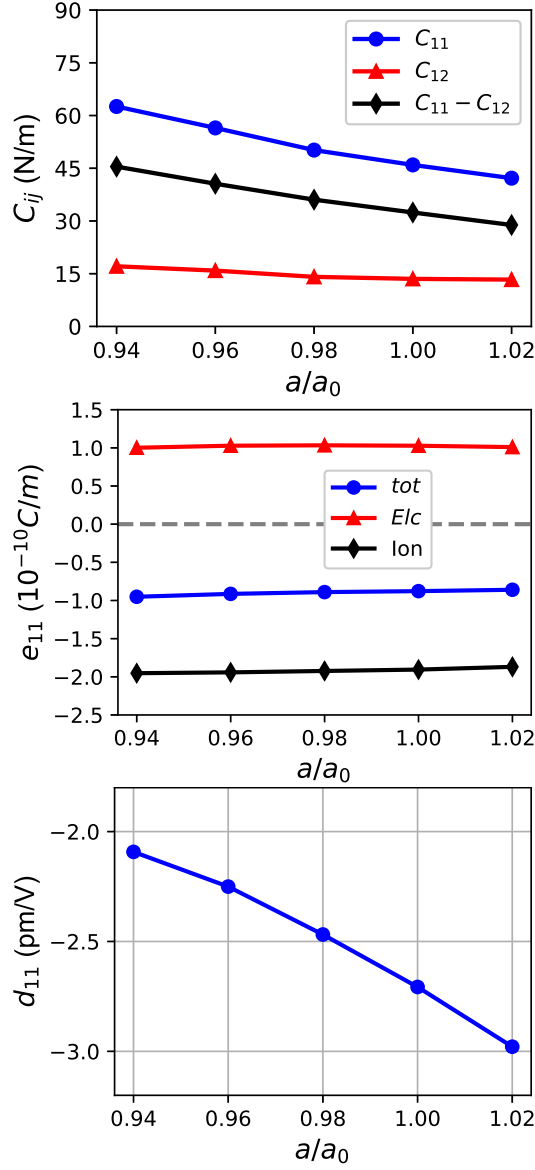


FIG. 9. (Color online) For monolayer GdCl₂, the elastic constants C_{ij} , the piezoelectric stress coefficient (e_{11}) along with the ionic contribution and electronic contribution, and the piezoelectric strain coefficient (d_{11}) with the application of biaxial strain (0.94 to 1.02).

of monolayer GdCl₂ in the 2D Brillouin zone without SOC and with SOC for magnetic moment of Gd along the positive and negative z direction are shown [Figure 5](#). Without SOC, the Berry curvatures of K and -K valleys are in opposite signs, and the absolute values are the same. When the SOC is included, their absolute values of the Berry curvatures of K and -K valleys are no longer identical, which shows the typical valley contrasting properties. It is also found that the numerical values between K and -K valleys overturn, when the magnetic moment of Gd changes from the positive to negative z direction.

TABLE I. For monolayer GdX₂ (X=F, Cl, Br and I), the elastic constants C_{ij} in Nm⁻¹, the piezoelectric stress coefficients e_{11} with electronic part e_{11e} and ionic part e_{11i} in 10⁻¹⁰ C/m, and the piezoelectric strain coefficients d_{11} in pm/V.

| Name | C_{11} | C_{12} | e_{11e} | e_{11i} | e_{11} | d_{11} |
|-------------------|----------|----------|-----------|-----------|----------|----------|
| GdF ₂ | 73.87 | 19.61 | 1.365 | -1.048 | 0.317 | 0.584 |
| GdCl ₂ | 45.95 | 13.53 | 1.028 | -1.906 | -0.878 | -2.708 |
| GdBr ₂ | 40.46 | 11.68 | 0.847 | -1.742 | -0.895 | -3.110 |
| GdI ₂ | 35.49 | 10.09 | 0.658 | -1.356 | -0.698 | -2.748 |

V. PIEZOELECTRIC PROPERTIES

The monolayer GdCl₂ with $\bar{p}6m2$ point-group symmetry lacks inversion symmetry, but the reflectional symmetry across the xy plane still holds. These mean that only e_{11}/d_{11} with defined x and y direction in [Figure 2](#) is nonzero. This is the same with ones of MoS₂ monolayer, but is different from ones of Janus monolayer MoSSe with additional e_{31}/d_{31} ³². For 2D materials, only considering the in-plane strain and stress³²⁻⁴⁰, the piezoelectric stress and strain tensors by using Voigt notation can be reduced into:

$$\begin{pmatrix} e_{11} & -e_{11} & 0 \\ 0 & 0 & -e_{11} \\ 0 & 0 & 0 \end{pmatrix} \quad (5)$$

$$\begin{pmatrix} d_{11} & -d_{11} & 0 \\ 0 & 0 & -2d_{11} \\ 0 & 0 & 0 \end{pmatrix} \quad (6)$$

When a uniaxial in-plane strain is imposed, the in-plane piezoelectric polarization ($e_{11}/d_{11} \neq 0$) can be induced. However, with an applied biaxial in-plane strain, the in-plane piezoelectric response will be suppressed ($e_{11}/d_{11} = 0$). The only independent d_{11} can be calculated by $e_{ik} = d_{ij}C_{jk}$:

$$d_{11} = \frac{e_{11}}{C_{11} - C_{12}} \quad (7)$$

We use the orthorhombic supercell (in [Figure 2](#)) to calculate the e_{11} of monolayer GdCl₂ with DFPT method. The calculated e_{11} is -0.878×10^{-10} C/m with ionic part -1.906×10^{-10} C/m and electronic part 1.028×10^{-10} C/m. The electronic and ionic polarizations have opposite signs, and the ionic contribution dominates the in-plane piezoelectricity. This is different from monolayer MoS₂, whose electronic and ionic contributions have the same sign, and the electronic part dominates the e_{11} ⁴⁰. Based on [Equation 7](#), the d_{11} can be calculated from previous calculated C_{ij} and e_{11} . The calculated d_{11} is -2.708 pm/V, which is comparable to one of α -quartz ($d_{11} = 2.3$ pm/V). The GdX₂ (X= Br and I) monolayers

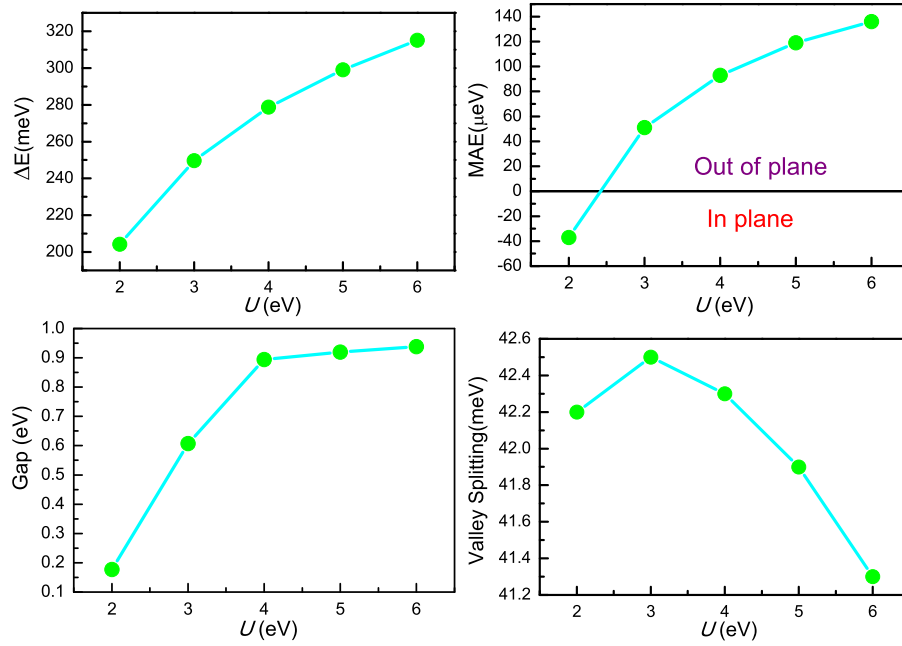


FIG. 10. (Color online) (Top left) The energy difference between the AFM and FM states (ΔE); (Top right) MAE; (Bottom left) energy band gap (Gap); (Bottom right) valley splitting as a function of U for monolayer GdCl_2 .

have been predicted^{19,20}, and they possess in-plane magnetic anisotropy. Here, we use GGA+ U_{eff} ($U_{eff} = 5.0$ and 8.0 eV for monolayer GdBr_2 and GdI_2 , respectively) method to investigate piezoelectric properties of GdX_2 ($X = \text{Br}$ and I) monolayers. The data related with elastic and piezoelectric properties are summarized in Table I. It is found that d_{11} of GdX_2 ($X = \text{Br}$ and I) monolayers are comparable with one of GdCl_2 .

VI. STRAIN EFFECTS

The VBM of unstrained monolayer GdCl_2 is at Γ point, and it is necessary to tune VBM to K/-K point by external field for practical applications. As is well known, the strain is a very effective method to tune the electronic structures of 2D materials^{41–47}. The a/a_0 is used to simulate the biaxial strain with a and a_0 being the strained and unstrained lattice constants. In considered strain range, to confirm the FM ground state, the energy differences of AFM with respect to FM state vs a/a_0 with rectangle supercell are plotted in Figure 6. It is found the energy difference with the biaxial strain varying from 0.94 to 1.06 is always positive, and monotonically decreases. This indicates that the ground state of monolayer GdCl_2 is FM in considered strain range, and the strain can strengthen the FM coupling between Gd atoms from tensile strain to compressive one. At applied strain, it is also very important to confirm PMA for stable long-range magnetic ordering without external field. For MAE, Figure 6 shows a decrease with increasing a/a_0 , and the MAE becomes negative value with the strain

over 1.03 , which means that the easy axis of monolayer GdCl_2 turns to in-plane.

We only show energy band structures of monolayer GdCl_2 (0.94 to 1.02) with PMA by using GGA+SOC in Figure 7, and the energy band gaps are plotted in Figure 6. At applied strain, monolayer GdCl_2 is always an indirect gap semiconductor. It is found that the compressive strain can induce the transition of VBM from Γ point to K/-K point, which can be observed at 0.98 strain. In fact, the change of VBM has been realized at only 0.99 strain, and the corresponding energy band is plotted in FIG.1 of electronic supplementary information (ESI). The tensile strain can make CBM change from M point to one point along Γ -M path. With a/a_0 from 0.94 to 1.02 , the energy band gap firstly increases, and then decreases, which can be observed in many 2D materials^{46,47}. As shown in Figure 6, the valley splitting increases monotonically with the increasing a/a_0 . Conversely, a compressive strain decreases the valley splitting, and the valley splitting will become negative value at about 0.963 strain, which implies that the energy of -K valley is higher than one of K valley. The Berry curvature distributions of monolayer GdCl_2 with a/a_0 being 0.94 , 0.98 and 1.02 by using GGA+SOC are shown in Figure 8. It is found that the Berry curvatures (absolute value) of two valleys become large with increasing a/a_0 .

It have been proved that strain engineering can effectively tune piezoelectric properties of 2D materials^{48–51}, and then we investigate the strain effects on piezoelectric properties of monolayer GdCl_2 . The elastic constants (C_{11} , C_{12} and $C_{11}-C_{12}$), piezoelectric stress coefficients (e_{11}) along the ionic and electronic contributions,

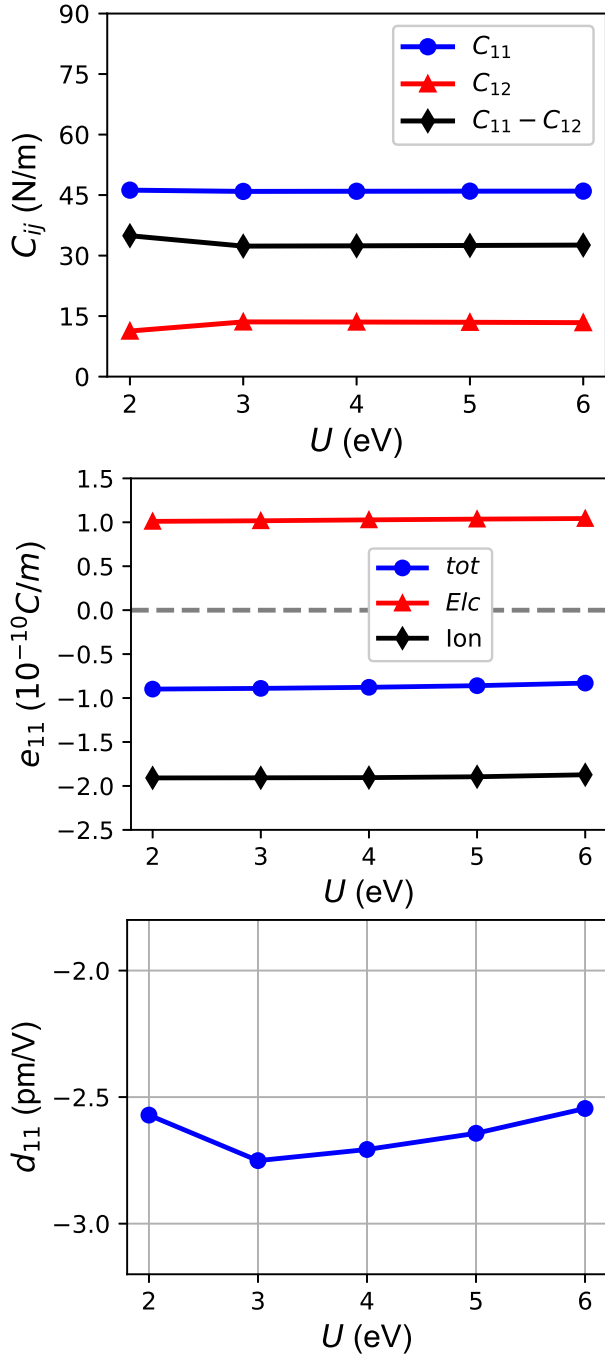


FIG. 11. (Color online) For monolayer GdCl_2 , the elastic constants C_{ij} , the piezoelectric stress coefficient (e_{11}) along with the ionic contribution and electronic contribution, and the piezoelectric strain coefficient (d_{11}) as a function of U .

and piezoelectric strain coefficients (d_{11}) of monolayer GdCl_2 as a function of a/a_0 are plotted in Figure 9. It is clearly seen that C_{11} , C_{12} and $C_{11}-C_{12}$ all decrease with increasing strain from 0.94 to 1.02 strain. In the considered strain range, the calculated elastic constants of strained monolayer GdCl_2 satisfy the mechanical stability criteria²⁹, so they are all mechanically stable. It

is found that the strain has little effects on e_{11} , including both the ionic and electronic contributions. However, with increasing a/a_0 , the d_{11} (absolute value) increases due to reduced $C_{11}-C_{12}$ based on Equation 7.

Considering various factors, very small compressive strain (about 0.99 strain) can make monolayer GdCl_2 to be a good valley material with PMA, VBM at K/-K point, strong FM coupling, proper valley splitting and d_{11} to realize PAVHE.

VII. ELECTRONIC CORRELATION EFFECTS

To further confirm the reliability of our results, the electronic correlation effects on magnetic, electronic and piezoelectric properties of monolayer GdCl_2 are investigated by choosing different U (2-6 eV). The energy differences between AFM and FM states with rectangle supercell and MAE vs U are plotted in Figure 10. With increasing U , the energy difference is always positive, and monotonically increases. These manifest that the monolayer GdCl_2 is always FM order, and the increasing U can strengthen the FM coupling between Gd atoms. The MAE shows a decrease with decreasing U , and the MAE becomes negative value with easy axis turning to in-plane with U being less than about 2.5 eV. The energy band structures of monolayer GdCl_2 ($U=2$ to 6 eV) by using GGA+SOC are plotted in FIG.2 of ESI, and the energy band gaps and valley splitting are plotted in Figure 10. When the U increases, the VBM is always at K/-K point, and the gap increases. It is found that the electronic correlation has little influence on valley splitting, and the change only 1.2 meV with different U (2-6 eV). From FIG.3 of ESI, the electronic correlation has little effects on Berry curvatures of K and -K valleys. The elastic constants (C_{11} , C_{12} and $C_{11}-C_{12}$), piezoelectric stress coefficients (e_{11}) along the ionic and electronic contributions, and piezoelectric strain coefficients (d_{11}) of monolayer GdCl_2 vs U are shown in Figure 11. Calculated results show that electronic correlation has small effects on d_{11} due to small influence on C_{ij} and e_{11} , and the change is about 0.21 pm/V.

VIII. DISCUSSION AND CONCLUSION

The GdX_2 (X=Cl, Br and I) monolayers have been predicted^{19,20}, and the easy axis of monolayer GdCl_2 is along the out of plane direction, while monolayer GdBr_2 and GdI_2 possess in-plane magnetic anisotropy. When the compressive strain is larger than 3%, the easy axis of monolayer GdBr_2 transfers from in-plane to out-of-plane²⁰. These mean that monolayer GdF_2 should have PMA due to small atomic radius of F atoms. For monolayer GdF_2 , the energy difference between AFM and FM is 0.285 eV, which means that the FM order is the ground state. The optimized lattice constants is 3.465 Å, and the calculated C_{11} and C_{12} are 73.87 Nm^{-1} and

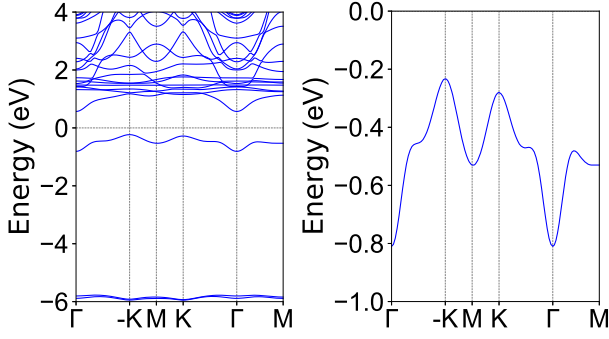


FIG. 12. (Color online) The band structure of monolayer GdF₂ with SOC for magnetic moment of Gd along the positive z direction (Left) with enlarged views of the valence bands near the Fermi level (Right).

19.61 Nm⁻¹, satisfying the Born criteria of mechanical stability²⁹. From FIG.4 of ESI, the monolayer GdF₂ is dynamically stable due to missing imaginary frequency. The PMA of monolayer GdF₂ is confirmed, and the corresponding MAE is 137 μ eV per Gd atom. The band structures of monolayer GdF₂ with SOC for magnetic moment of Gd along the positive z direction are plotted in Figure 12. The monolayer GdF₂ is an indirect gap semiconductor (0.80 eV) with VBM at K/-K point and CBM at Γ point. It is found that the energy of -K valley is higher than one of K valley with valley splitting of 47.6 meV. Calculated Berry curvature distribution of monolayer GdF₂ with SOC for magnetic moment of Gd along the positive z direction is plotted in FIG.5 of ESI. The absolute values of the Berry curvatures of K and -K valleys are smaller than ones of monolayer GdCl₂, and are no longer identical with the typical valley contrasting properties. Finally, the piezoelectric properties of

monolayer GdF₂ are investigated, and the calculated d_{11} is 0.584 pm/V. With respect to GdX₂ (X=Cl, Br and I) monolayers, the d_{11} of monolayer GdF₂ becomes positive, which is because the electronic part of monolayer GdF₂ is larger than ionic one. The related data are summarized in Table I. These results show that monolayer GdF₂ may be a potential valley material to achieve PAVHE.

In summary, a possible way is proposed to achieve anomalous valley Hall effect by piezoelectric effect, and then the valleytronic and piezoelectric properties of monolayer GdCl₂ are investigated by the reliable first-principle calculations. Monolayer GdCl₂ is a FM semiconductor with a pair of valleys locating at the K and -K points, and possess PMA. Arising from the intrinsic magnetic interaction, broken inversion symmetry and SOC, the valley splitting can be observed between K and -K valleys, and the corresponding value is 42.3 meV. The predicted d_{11} is -2.708 pm/V, which can provide a suitable in-plane electric field by uniaxial in-plane strain. Moreover, the effects of strain and electronic correlation on the valley physics and piezoelectric properties are also studied. Finally, a 2D FM semiconductor GdF₂ is predicted, which is also a potential ferrovalley material. Our work provides an initial idea for realizing and manipulating the valley physics.

ACKNOWLEDGMENTS

This work is supported by Natural Science Basis Research Plan in Shaanxi Province of China (2021JM-456). We are grateful to the Advanced Analysis and Computation Center of China University of Mining and Technology (CUMT) for the award of CPU hours and WIEN2k/VASP software to accomplish this work.

- ¹ J. R. Schaibley, H. Yu, G. Clark, P. Rivera, J. S. Ross, K. L. Seyler, W. Yao, and X. Xu, Nat. Rev. Mater. **1**, 16055 (2016).
- ² D. Xiao, G. B. Liu, W. Feng, X. Xu, and W. Yao, Phys. Rev. Lett. **108**, 196802 (2012).
- ³ S. A. Vitale, D. Nezich, J. O. Varghese, P. Kim, N. Gedik, P. Jarillo-Herrero, D. Xiao, and M. Rothschild, Small **14**, 1801483 (2018).
- ⁴ G. Pacchioni, Nat. Rev. Mater. **5**, 480 (2020).
- ⁵ W. Yao, D. Xiao, and Q. Niu, Phys. Rev. B **77**, 235406 (2008).
- ⁶ D. Xiao, W. Yao, and Q. Niu, Phys. Rev. Lett. **99**, 236809 (2007).
- ⁷ Z. Zhu, A. Collaudin, B. Fauqué, W. Kang, and K. Behnia, Nat. Phys. **8**, 89 (2012).
- ⁸ M. N. Blonsky, H. L. Zhuang, A. K. Singh and R. G. Hennig, ACS Nano, **9**, 9885 (2015).
- ⁹ D. Xiao, M. C. Chang, and Q. Niu, Rev. Mod. Phys. **82**, 1959 (2010).
- ¹⁰ W. Y. Tong, S. J. Gong, X. Wan, and C. G. Duan, Nat. Commun. **7**, 13612 (2016).
- ¹¹ Y. B. Liu, T. Zhang, K. Y. Dou, W. H. Du, R. Peng, Y. Dai, B. B. Huang, and Y. D. Ma, J. Phys. Chem. Lett. **12**, 8341 (2021).
- ¹² Z. Song, X. Sun, J. Zheng, F. Pan, Y. Hou, M.-H. Yung, J. Yang, and J. Lu, Nanoscale **10**, 13986 (2018).
- ¹³ J. Zhou, Y. P. Feng, and L. Shen, Phys. Rev. B **102**, 180407(R) (2020).
- ¹⁴ P. Zhao, Y. Ma, C. Lei, H. Wang, B. Huang, and Y. Dai, Appl. Phys. Lett. **115**, 261605 (2019).
- ¹⁵ X. Y. Feng, X. L. Xu, Z. L. He, R. Peng, Y. Dai, B. B. Huang and Y. D. Ma, Phys. Rev. B **104**, 075421 (2021).
- ¹⁶ Y. Zang, Y. Ma, R. Peng, H. Wang, B. Huang, and Y. Dai, Nano Res. **14**, 834 (2021).
- ¹⁷ R. Peng, Y. Ma, X. Xu, Z. He, B. Huang, and Y. Dai, Phys. Rev. B **102**, 035412 (2020).
- ¹⁸ W. Du, Y. Ma, R. Peng, H. Wang, B. Huang, and Y. Dai, J. Mater. Chem. C **8**, 13220 (2020).
- ¹⁹ B. Wang, X. W. Zhang, Y. H. Zhang, S. J. Yuan, Y. L. Guo, S. Dong and J. L. Wang, Mater. Horiz. **7**, 1623 (2020).
- ²⁰ W. Q. Liu, J. W. Tong, L. Deng, B. Yang, G. M. Xie, G.

- W. Qin, F. B. Tian, X. M. Zhang, *Materials Today Physics* **21**, 100514 (2021).
- ²¹ H. X. Cheng, J. Zhou, W. Ji, Y. N. Zhang and Y. P. Feng, *Phys. Rev. B* **103**, 125121 (2021).
 - ²² P. Hohenberg and W. Kohn, *Phys. Rev.* **136**, B864 (1964); W. Kohn and L. J. Sham, *Phys. Rev.* **140**, A1133 (1965).
 - ²³ G. Kresse, *J. Non-Cryst. Solids* **193**, 222 (1995).
 - ²⁴ G. Kresse and J. Furthmüller, *Comput. Mater. Sci.* **6**, **15** (1996).
 - ²⁵ G. Kresse and D. Joubert, *Phys. Rev. B* **59**, 1758 (1999).
 - ²⁶ J. P. Perdew, K. Burke and M. Ernzerhof, *Phys. Rev. Lett.* **77**, 3865 (1996).
 - ²⁷ X. Wu, D. Vanderbilt and D. R. Hamann, *Phys. Rev. B* **72**, 035105 (2005).
 - ²⁸ A. Togo, F. Oba, and I. Tanaka, *Phys. Rev. B* **78**, 134106 (2008).
 - ²⁹ E. Cadelano and L. Colombo, *Phys. Rev. B* **85**, 245434 (2012).
 - ³⁰ C. Lee, X. Wei, J. W. Kysar and J. Hone, *Science* **321**, 385 (2008).
 - ³¹ T. Fukui, Y. Hatsugai and H. Suzuki, *J. Phys. Soc. Japan* **74**, 1674 (2005).
 - ³² L. Dong, J. Lou and V. B. Shenoy, *ACS Nano*, **11**, 8242 (2017).
 - ³³ R. X. Fei, W. B. Li, J. Li and L. Yang, *Appl. Phys. Lett.* **107**, 173104 (2015).
 - ³⁴ M. N. Blonsky, H. L. Zhuang, A. K. Singh and R. G. Hennig, *ACS Nano*, **9**, 9885 (2015).
 - ³⁵ Y. Chen, J. Y. Liu, J. B. Yu, Y. G. Guo and Q. Sun, *Phys. Chem. Chem. Phys.* **21**, 1207 (2019).
 - ³⁶ S. D. Guo, Y. T. Zhu, W. Q. Mu and W. C. Ren, *EPL* **132**, 57002 (2020).
 - ³⁷ S. D. Guo, Y. T. Zhu, W. Q. Mu, L. Wang and X. Q. Chen, *Comp. Mater. Sci.* **188**, 110223 (2021).
 - ³⁸ Y. Guo, S. Zhou, Y. Z. Bai, and J. J. Zhao, *Appl. Phys. Lett.* **110**, 163102 (2017).
 - ³⁹ W. B. Li and J. Li, *Nano Res.* **8**, 3796 (2015).
 - ⁴⁰ K. N. Duerloo, M. T. Ong and E. J. Reed, *J. Phys. Chem. Lett.* **3**, 2871 (2012).
 - ⁴¹ K. L. He, C. Poole, K. F. Mak and J. Shan, *Nano Lett.* **13**, 2931 (2013).
 - ⁴² H. L. Shi, H. Pan, Y. W. Zhang and B. I. Yakobson, *Phys. Rev. B* **87**, 155304 (2013).
 - ⁴³ T. Cheiwchanchamnangij, W. R. L. Lambrecht, Y. Song and H. Dery, *Phys. Rev. B* **88**, 155404 (2013).
 - ⁴⁴ H. Y. Lv, W. J. Lu, D. F. Shao, H. Y. Lub and Y. P. Sun, *J. Mater. Chem. C* **4**, 4538 (2016).
 - ⁴⁵ H. Peelaers and C. G. Van de Walle, *Phys. Rev. B* **86**, 241401(R) (2012).
 - ⁴⁶ S. D. Guo and J. Dong, *Semicond. Sci. Tech.* **33**, 085003 (2018).
 - ⁴⁷ S. D. Guo, *J. Mater. Chem. C* **4**, 9366 (2016).
 - ⁴⁸ N. Jena, Dimple, S. D. Behere and A. D. Sarkar, *J. Phys. Chem. C* **121**, 9181 (2017).
 - ⁴⁹ S. D. Guo, X. S. Guo, Y. Y. Zhang and K. Luo, *J. Alloy. Compd.* **822**, 153577 (2020).
 - ⁵⁰ Dimple, N. Jena, A. Rawat, R. Ahammed, M. K. Mohanta and A. D. Sarkar, *J. Mater. Chem. A* **6**, 24885 (2018).
 - ⁵¹ S. D. Guo, W. Q. Mu and Y. T. Zhu, *J. Phys. Chem. Solids* **151**, 109896 (2021).